Effect of Prestage Hydrothermal Treatment on the Formation of Struvite vs Vivianite during Semicontinuous Anaerobic Digestion of Sewage Sludge

Qian Wang, Xiaoguang Liu, Haesung Jung, Simin Zhao, Spyros G. Pavlostathis, and Yuanzhi Tang*

ACCESS | Metrics & More | Article Recommendations | SI Supporting Information

ABSTRACT: Anaerobic digestion (AD) with prestage hydrothermal treatment (HT) is an emerging strategy for the sustainable management of sewage sludge and recovery of valuable resources. Both struvite and vivianite can be precipitated during AD process and serve as two important phases for phosphorus (P) and/or nitrogen (N) recovery. Yet the effect of HT conditions on the phase selection and precipitation of struvite vs vivianite in the subsequent AD process remains unclear. This study investigated the evolution and mineralization of P and N in sewage sludge during AD with prestage HT using complementary chemical extraction and X-ray spectroscopy characterizations. Influencing factors such as sludge type and HT temperature were explored. For raw sludge with high molar ratio of Mg/Fe (5.9), HT did not induce the formation of struvite in the HT-derived hydrochars, because the acidic pH of HT slurries was similar to that in the raw sludge. Struvite was observed during the AD of low temperature (90 and 125 °C) HT slurries due to the reaction of Mg-phosphate phases with high concentration of NH_4^+ at pH > 7. For HT slurries prepared at 155 °C, the pH was always below 7 during the subsequent AD process, preventing struvite precipitation in the AD solids. For raw sludge with low molar ratio of Mg/Fe (1.1), HT at 90 and 125 °C induced the formation of vivianite in the hydrochars, as compared to the formation of strengite at 155 °C HT. In comparison with the corresponding hydrochars, more vivianite was precipitated during the subsequent AD via microbial reduction of Fe(III) species. Results from this study suggest that the formation of struvite or vivianite in the final AD solids is highly dependent on the Mg/Fe molar ratio and/or the pH of AD suspensions. Meanwhile, both HT and AD also strongly affected N speciation evolution in sewage sludge. Along with the release of large amounts of ammonia, HT favored the accumulation of quaternary- and pyrrole-N in the hydrochars, while only pyrrole-N was enriched in the AD solids. This study sheds light on the recycling and reclamation of P and N during HT-AD of sewage sludge.

KEYWORDS: Struvite, Vivianite, Phosphorus, Nitrogen, Resource recovery, Anaerobic digestion, Hydrothermal treatment
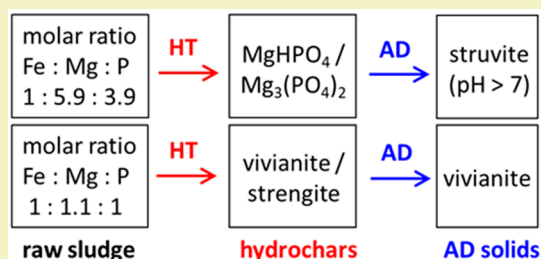
INTRODUCTION

More than 10 million dry tons of sewage sludge are generated annually as a byproduct of publicly owned municipal wastewater treatment works in the United States. Sewage sludge generally consists of a significant portion of organic matter (OM), phosphorus (P), and nitrogen (N),[1−3] providing great opportunities for energy recovery via biomethane production and recycling/reclamation of nutrients.[1,4−7] However, sewage sludge also contains toxic metals (e.g., Cu, Zn, and Cr) and organic pollutants (e.g., polycyclic aromatic hydrocarbons (PAHs) and polychlorinated dibenzofurans (PCDFs)), along with pathogenic bacteria.[8−10] Thus, the management of sewage sludge must integrate resource recovery and safe disposal to achieve societal and environmental sustainability.

Anaerobic digestion (AD) is the most common technique to produce biomethane from sewage sludge via the degradation of complex OM. AD can also reduce sludge mass, remove odor, inactivate pathogens, and improve sludge dewaterability.[11−13]

AD performs in a series of steps, including hydrolysis, acidogenesis, acetogenesis, and methanogenesis.[14] For particulate OM, hydrolysis is the rate-limiting step in the overall AD process; it refers to the solubilization and transformation of particulate OM into more bioavailable and fermentable substrates for the subsequent steps.[14,15] In recent years, to improve AD performance and enhance sludge biodegradation and biomethane production, AD with prestage hydrothermal treatment (HT) (i.e., sequential HT-AD) has emerged as a sustainable technique for sludge management[16,17] and energy recovery.[18,19]
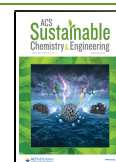
In addition to the benefits of energy recovery, AD provides the opportunity for the recovery of nutrients such as P and N. Two important mineral phases, vivianite ($Fe_2(PO_4)_3 \cdot 8H_2O$) and struvite ($MgNH_4PO_4 \cdot 6H_2O$), are commonly found in anaerobic digestate and can serve for P/N recovery.[1,20] An understanding of their formation conditions and influencing factors can facilitate the design/selection of downstream processing/application options of the treatment products (i.e., vivianite and struvite). Vivianite is the main phosphate mineral in anaerobic digestate,[20−23] as Fe salts are widely used for phosphate removal and as coagulants in water resource recovery facilities (WRRFs).[22,24] Vivianite from anaerobic digestate can be recovered via microbial electrolysis cell[25] or magnetic separation.[20] Struvite can also precipitate in anaerobic digestate from wastewater treatment plants with enhanced biological phosphorus removal (EBPR).[26−28] Considering that ∼55% of all sludge produced in the United States is land applied,[29] struvite as an excellent slow release P fertilizer[30] might enhance soil nutrient input and improve crop yield. However, the presence of Fe and Ca can interfere with struvite precipitation in anaerobic digestate, due to the strong affinity of P to Fe[31] and the formation of Ca phosphate minerals such as hydroxyapatite (HAP).[32,33]

For sequential HT-AD, the formation of vivianite vs struvite at each step (i.e., HT hydrochar and final AD solids) and the influencing factors are poorly understood. For vivianite, our recent study showed that HT of sewage sludge (with a P/Fe ratio of 2.1) at 90 °C favored vivianite formation in the hydrochars, whereas HT at 155 and 185 °C inhibited the precipitation of vivianite during the subsequent AD (batch assay, 79 d).[34] It is unclear whether similar transformation of P and Fe in sewage sludge would occur in the HT-AD process in a semicontinuously fed AD system at different solids retention times (SRTs), which is the most commonly employed setting in WRRFs.[35] For struvite, a few previous studies showed that it did not readily precipitate in hydrochars during HT of animal manure, activated sludge, or mixture of primary and activated sludges, due to the acidic conditions (pH ≤ 6) of the slurries derived from HT at 90−300 °C and/or the presence of Fe and Ca.[34,36−38] Wet decomposition of struvite can occur at even 39.5 °C,[39,40] further decreasing its likelihood of formation during HT. However, Bayuseno and Schmahl[41] synthesized struvite under hydrothermal conditions at 60−120 °C with an initial pH of 7−10. The possibility of struvite formation during HT of sludge with high Mg content has not been clarified, which warrants further investigation. Few studies have investigated the precipitation of struvite in sewage sludge during sequential HT-AD with semicontinuous AD operation.

This study aims to fill the knowledge gaps on the roles of sludge composition (e.g., metal types and contents), prestage HT temperature, and semicontinuous AD operation with different SRTs on the formation of vivianite and/or struvite during sequential HT-AD.

■ MATERIALS AND METHODS

A sludge mixture of primary sludge (PS) and waste activated sludge (WAS) was used, as they are typically mixed and fed to on-site AD in most WRRFs.[42] On the basis of the chemical formula of vivianite and struvite, Fe and Mg are two important metal cations to consider. Thus, raw sludge mixture with different initial molar ratios of Mg/Fe (5.9 and 1.1) was collected from the same WRRF with EBPR. For both sludges, prestage HT was conducted at 90, 125, or 155 °C, representing different sludge hydrolysis conditions/rates,[34] followed by semicontinuous AD with different SRTs. The raw sludge solids,

HT hydrochars, and AD solids at different digestion times were systematically characterized using chemical extraction, X-ray diffraction (XRD), P K-edge X-ray absorption near edge structure (XANES) spectroscopy, and X-ray photoelectron spectroscopy (XPS) to reveal the speciation and mineralogy of P and N.

Sample Collection. Sludge samples and digestate were collected from the F. Wayne Hill Water Resources Center in Buford, GA, USA. The Center employs EBPR process without Fe dosing. The internal P of the sludge mixture is removed by a Waste Activated Sludge Stripping unit, and the released P in the filtrate is recovered by a rotary drum thickener where the sludge mixture is also thickened. The thickened sludge is finally fed to a mesophilic (35 °C) anaerobic digester.

The thickened sludge (a mixture of PS and WAS) was collected twice from the Center and used for the experiments of HT-AD with semicontinuous AD operation at different SRTs. For the experiments with 10 d SRT (i.e., HT-AD with 10 d SRT system), the sludge mixture has a Mg/Fe molar ratio of 5.9 and water content of 93.7%. For experiments with 20 d SRT (i.e., HT-AD with 20 d SRT system), the Mg/Fe ratio was 1.1 and water content of 94.8%. The physicochemical properties of these two sludge mixtures can differ due to the changes of wastewater feed and operational conditions. Digestate was also collected from the Center and was anaerobically incubated at 35 °C in the lab until no significant biomethane production, serving as the anaerobic inoculum. Our companion paper[43] assessed two SRTs (10 and 20 d) in terms of AD performance and energy balance while this study focuses on the formation of vivianite and struvite during HT-AD with semicontinuous AD setting.

HT-AD Treatment. For HT, 130 mL of sludge mixture was loaded to a 200 mL polypropylene-lined stainless-steel hydrothermal reactor (COL-INT TECH., Irmo, SC, USA). Six replicate reactors were tightly sealed and heated in a forced air oven at the target temperature (90, 125, or 155 °C) for 4 h (3 h ramping and 1 h holding) and then cooled down to room temperature naturally. Note that the hydrothermal reactor used in this study took ∼3 h to reach the target temperature (90−185 °C) as described in detail in our previous study.[44] The HT slurries were collected at the end of each treatment and stored in glass bottles at 4 °C in the dark until used for the subsequent AD. In addition, a portion of HT slurries were separated by centrifugation into the solids (hereinafter hydrochars, although HT at 90 and 125 °C does not readily converts biomass to chars) and liquid (hereinafter HT process water)

The subsequent semicontinuous AD experiments were conducted in 2.8 L water-jacketed Spinner cell flasks (Bellco Glass, Inc., Vineland, NJ, USA) (1 L working volume) mixed with a magnet-bearing Teflon mixer assembly at 35 °C. The anaerobic digesters started with the anaerobic inoculum, and then the HT slurries derived from each HT treatment were fed to each anaerobic digester. For AD experiments using raw sludge with a Mg/Fe molar ratio of 5.9, the nominal SRT and organic loading rate (OLR) were 10 d and 7.0 g total COD/L-d, respectively. The AD process lasted over 30 d (3 retention times). For AD experiments using raw sludge with a Mg/Fe ratio of 1.1, the SRT, OLR, and AD duration were 20 d, 3.5 g total COD/L-d, and 62 d (3 retention times). The feeding cycle was 2−3 d for both systems. The two raw sludges without HT were anaerobically incubated following the same procedures with 10 and 20 d SRT as the control experiments. During AD, a portion of the slurries was collected at certain time points and immediately centrifuged to separate the solids (hereinafter AD solids) and liquid (hereinafter AD process water). In addition, a portion of the raw sludges without any treatment were separated into solids and supernatants by centrifugation.

The obtained HT hydrochars and AD solids as well as raw sludge solids were freeze-dried under a vacuum. The HT and AD process waters as well as raw sludge supernatants were passed through 0.45 μm membrane filters. All dried solids were finely ground and stored in a COY anaerobic chamber (95% N_2/5% H_2; COY Lab) prior to characterization (details below). The biomethane volume produced was monitored periodically, which was reported in our recent parallel

Table 1. Sample Labels and Reaction Conditions of Hydrothermal Treatment (HT) and Anaerobic Digestion (AD) Processes[a]

System	Sample label*	Treatment	Reaction condition
HT-AD with 10 d SRT (molar ratio of Fe: Mg: P = 1: 5.9:3.9)	S10		Raw sludge, pH 5.71
	S10A10	AD	AD of S10, 35 °C, 10 d, pH 7.41
	S10A20	AD	AD of S10, 35 °C, 20 d, pH 7.31
	S10A30	AD	AD of S10, 35 °C, 30 d, pH 7.38
	S10H90	HT	HT treatment of S10 slurries, 90 °C, 4 h, pH 5.89
	S10H90A10	HT-AD	AD of S10H90-derived slurries, 35 °C, 10 d, pH 7.40
	S10H90A20	HT-AD	AD of S10H90-derived slurries, 35 °C, 20 d, pH 7.32
	S10H90A30	HT-AD	AD of S10H90-derived slurries, 35 °C, 30 d, pH 7.34
	S10H125	HT	HT treatment of S10 slurries, 125 °C, 4 h, pH 5.68
	S10H125A10	HT-AD	AD of S10H125-derived slurries, 35 °C, 10 d, pH 7.48
	S10H125A20	HT-AD	AD of S10H125-derived slurries, 35 °C, 20 d, pH 7.32
	S10H125A30	HT-AD	AD of S10H125-derived slurries, 35 °C, 30 d, pH 7.38
	S10H155	HT	HT treatment of S10 slurries, 155 °C, 4 h, pH 5.50
	S10H155A10	HT-AD	AD of S10H155-derived slurries, 35 °C, 10 d, pH 7.02
	S10H155A20	HT-AD	AD of S10H155-derived slurries, 35 °C, 20 d, pH 6.97
	S10H155A30	HT-AD	AD of S10H155-derived slurries, 35 °C, 30 d, pH 6.99
HT-AD with 20 d SRT (molar ratio of Fe: Mg: P = 1: 1.1:1)	S20		Raw sludge, pH 7.44
	S20A32	AD	AD of S20, 35 °C, 32 d, pH 7.67
	S20A62	AD	AD of S20, 35 °C, 62 d, pH 7.65
	S20H90	HT	HT treatment of S20 slurries, 90 °C, 4 h, pH 7.54
	S20H90A32	HT-AD	AD of S20H90-derived slurries, 35 °C, 32 d, pH 7.70
	S20H90A62	HT-AD	AD of S20H90-derived slurries, 35 °C, 62 d, pH 7.63
	S20H125	HT	HT treatment of S20 slurries, 125 °C, 4 h, pH 7.38
	S20H125A32	HT-AD	AD of S20H125-derived slurries, 35 °C, 32 d, pH 7.62
	S20H125A62	HT-AD	AD of S20H125-derived slurries, 35 °C, 62 d, pH 7.65
	S20H155	HT	HT treatment of S20 slurries, 155 °C, 4 h, pH 7.24
	S20H155A32	HT-AD	AD of S20H155-derived slurries, 35 °C, 32 d, pH 7.74
	S20H155A62	HT-AD	AD of S20H155-derived slurries, 35 °C, 62 d, pH 7.67

[a]Note: The sample label consists of "Sludge (S)", "HT-AD with 10 or 20 d SRT system (10 or 20)", "HT at 90, 125, or 155 °C (H90, H125, or H155)", and/or "AD at 10, 20, 30, 32, 62 d (A10, A20, A30, A32, or A62)".

study.[43] Sample labels and treatment conditions are provided in Table 1.

Characterization of Reaction Products. A portion of the raw sludge solids, HT hydrochars, and AD solids were digested by aqua regia. Briefly, ~0.2 g dried solids were ashed at 550 °C in a furnace for 2 h, followed by aqua regia digestion on a plate at 150 °C for 4 h. Major metal concentrations of the digested solids, raw sludge supernatants, and HT and AD process waters were analyzed by inductively coupled plasma-mass spectrometry (ICP-MS; Agilent 7500a). Total P concentration was measured as orthophosphate using the molybdate-ascorbic method[45] on an UV−vis spectrophotometer (Carey 60, Agilent). Bioavailable P (soluble and exchangeable P) in the solid samples was extracted using 0.5 M NaHCO$_3$[46] and analyzed as orthophosphate. The P species remained in the solid samples after the extraction were defined as insoluble P. The total N content in the solids was determined using Micro-Dumas combustion analysis on a Carlo Erba NA1500 Nitrogen/Carbon/Sulfur Analyzer. The concentration of NH$_4^+$ in supernatants, process waters, and solid samples (extracted by 2 M KCl; representing the soluble and exchangeable N)[47] was determined using the phenate method[47] on the UV−vis spectrophotometer.

Solid samples were analyzed by XRD, P K-edge XANES spectroscopy, and N 1s XPS. XRD analysis used a zero-background sample holder. Data collection was conducted on a PANalytical Empyrean X-ray diffractometer (Cu Kα radiation), with a scan step of 0.013° at 1° min^{-1} in the 2θ range of 5−70°.

P K-edge XANES spectra were collected in fluorescence mode using a PIPS detector at Beamline 14−3 at the Stanford Synchrotron Radiation Lightsource (SSRL), Menlo Park, CA, USA. Finely ground solid powders were spread evenly on the adhesive side of P-free Kapton tapes, and the sample chamber was kept under He atmosphere at room temperature. Energy calibration used AlPO$_4$

(edge position 2152.8 eV). XAS data analysis used the software Ifeffit.[48] For P XANES spectra, principal component analysis (PCA) and target transformation (TT) were performed on the spectra to determine the number of member components and identify candidate P species for the subsequent linear combination fitting (LCF) analysis. LCF analysis of the XANES spectra was conducted at energy range of −20 to +60 eV relative to the edge energy to quantify the P species in the solid samples. Goodness of fitting was evaluated using the residual factor (R-factor). Fits with the smallest R-factors were reported.

It is difficult to fit complex and heterogeneous sludge samples using one or a few P standard compounds. As Mg, Fe, Al, and/or Ca are major metals present in raw sludges, phosphate could either precipitate with these metals or adsorb on their metal mineral phases. Thus, a set of P standard compounds were used for LCF analysis, including (1) phytic acid (PhyAc), representing organic phosphate; (2) struvite, MgHPO$_4$, and Mg$_3$(PO$_4$)$_2$, representing Mg-associated P; (3) vivianite, strengite (FePO$_4$·2H$_2$O), and phosphate-adsorbed ferrihydrite (P-Ferrihy), representing Fe-associated P; (4) AlPO$_4$ and phosphate sorbed on Al$_2$O$_3$ (P−Al$_2$O$_3$), representing Al-associated P; and (5) brushite, hydroxyapatite (HAP), amorphous calcium phosphate (ACP), and octacalcium phosphate (OCP), representing Ca-associated P. These standard compounds used in this study have been shown to well represent P species in sludge samples.[3,34,49−51] Details on these standard compounds were presented in Table S1 and Figure S1.

N 1s XPS data were collected using a K-alpha XPS system (Thermo Fisher Scientific) with an Al K-alpha 1.486 keV source. The C 1s peak (284.6 eV) was used as the energy reference. The spectra were fitted using the software Thermo Avantage and deconvoluted into the following five peaks: 399.5 ± 0.1 eV (amine-N), 399.9 ± 0.1 eV (amino-N), 400.4 ± 0.1 eV (pyrrolic-N), 401.4 ± 0.1 eV
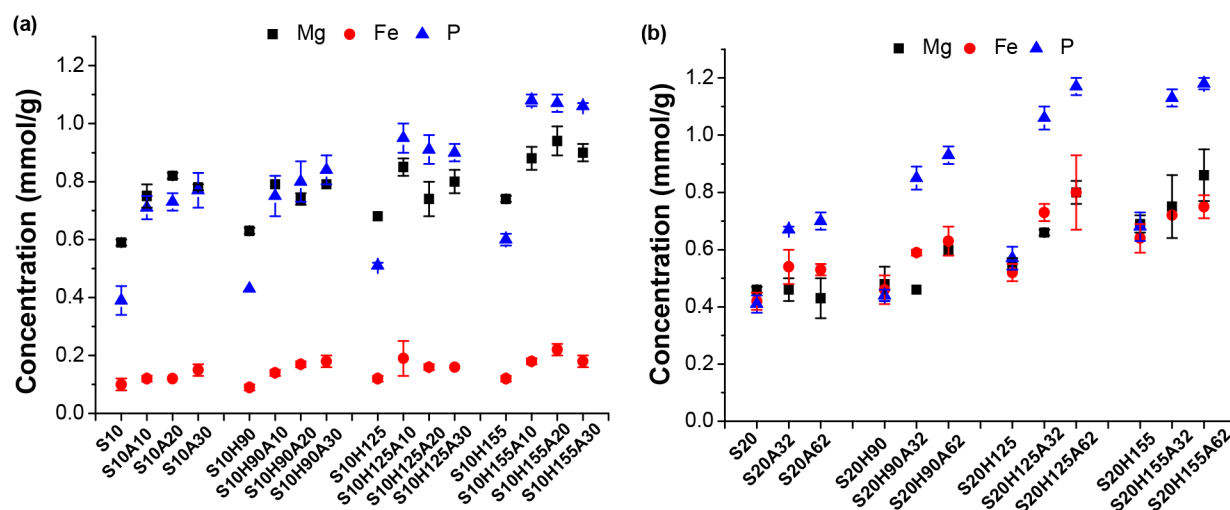
Figure 1. Total concentrations of Mg, Fe, and P in the solid samples. (a) HT-AD with 10 d SRT system; (b) HT-AD with 20 d SRT system.
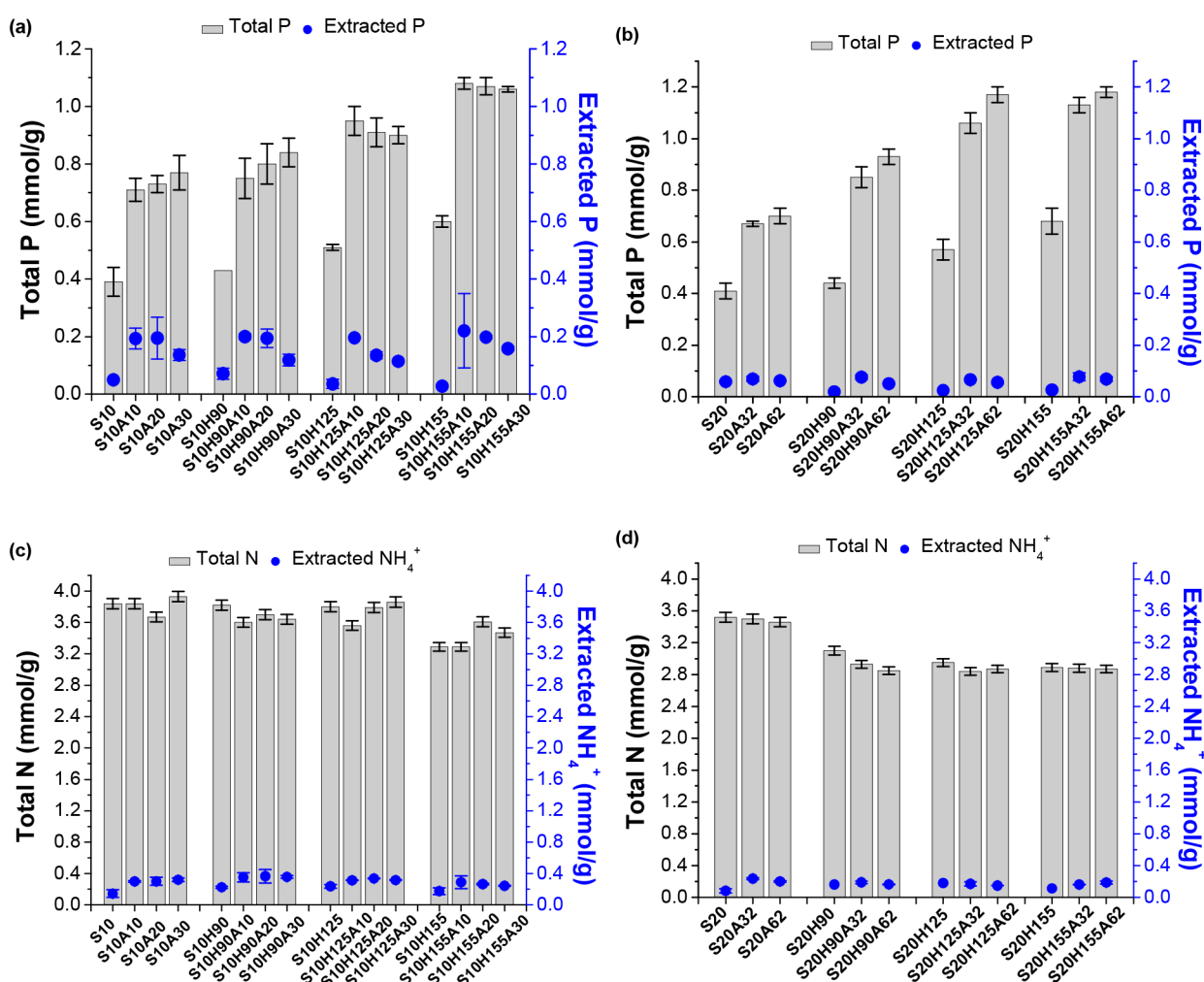

Figure 2. Total concentrations of P and N and extracted P and NH_4^+ in the solid samples. (a, c) are HT-AD with 10 d SRT system; (b, d) are HT-AD with 20 d SRT system.

(quarternary-N),[52] and 402.5 ± 0.1 eV (inorganic N).[4] The curve resolution process was described in Kelemen et al.[52,53] Briefly, the signal was curve-resolved using a 70% Gaussian, 30% Lorentzian line shape, and the peak position and full width at half-maximum (fwhm)

(1.7 eV) were fixed for each N fraction. This provided the best fit with
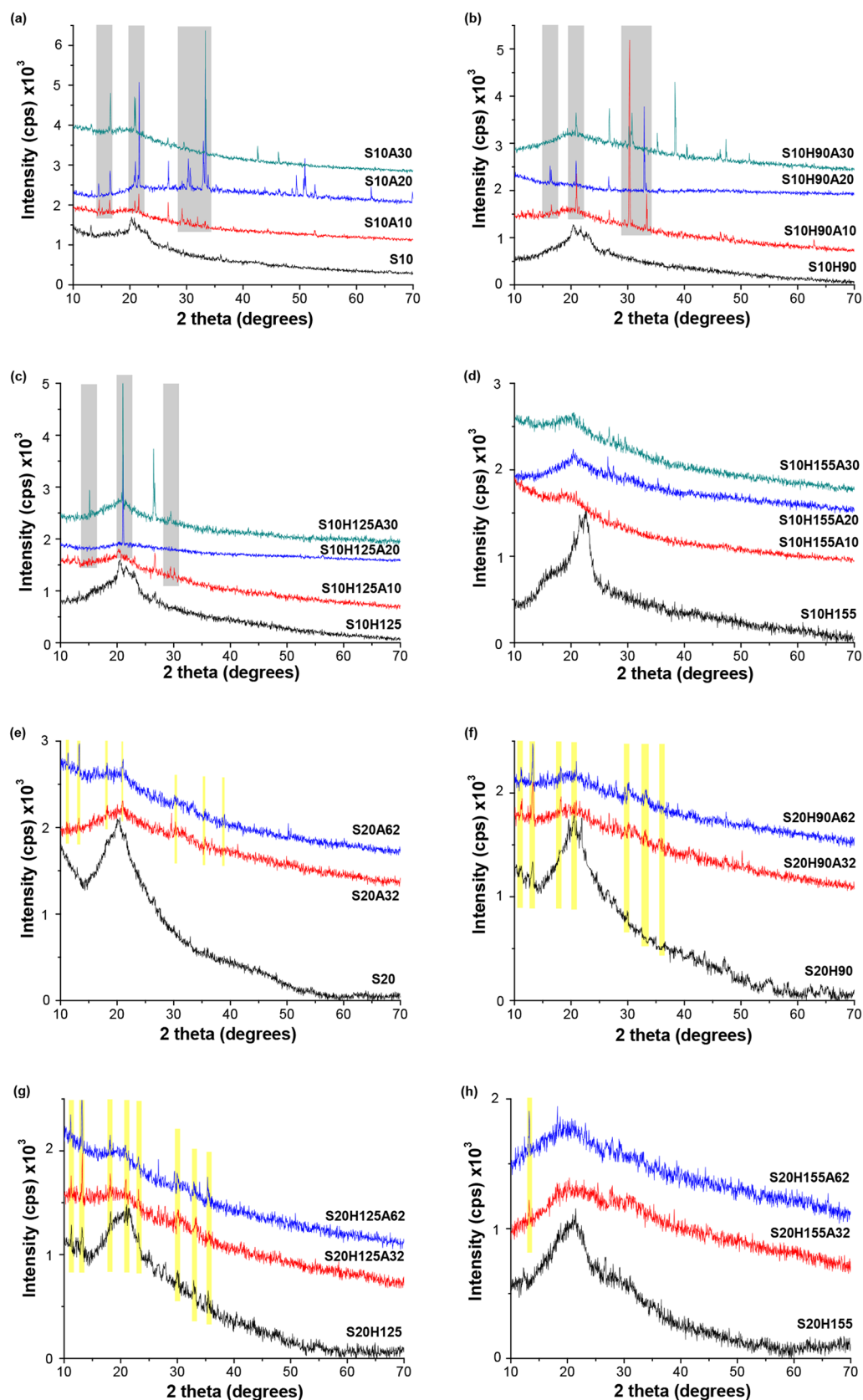
3% of standard deviation at a 95% confidence level.

Figure 3. XRD patterns of the raw sludges, HT hydrochars, and AD solids. Gray and yellow vertical bars indicate XRD peak positions for struvite (PDF no. 15−0762) and vivianite (PDF no. 83−2453), respectively. (a−d) HT-AD with 10 d SRT system; (e−h) HT-AD with 20 d SRT system.

RESULTS AND DISCUSSION

Chemical Characteristics of Solid and Liquid Samples. The major elemental composition in the raw sludge solids, HT hydrochars, AD solids, raw sludge supernatants, HT process water, and AD process water are shown in Figures 1 and 2 and Tables S2 and S3. For HT-AD with 10 d SRT system, the concentrations of Mg, Fe, Al, Ca, and P in solid sample S10 are 0.59, 0.10, 0.27, 0.22, and 0.39 mmol/g, respectively. The concentrations of Mg, Al, Ca, and P in the hydrochars increased with increasing HT temperature. This is consistent with our previous studies showing that HT enriched metals and P in the hydrochars.[34,49] However, HT did not increase Fe concentration in the hydrochars significantly. It was probably due to the much lower concentration of Fe than those of Mg and Al in the raw sludge. For the metal concentrations in HT process water, it slightly increased as compared to those in S10 supernatant. Especially, the concentration of Mg in sample S10H155 was 5.73 mmol/L, much higher than that in S10 supernatant (0.14 mmol/L). For P concentration in the HT process water, it increased from 0.16 (S10) to 0.47 (S10H125) mmol/L with increasing HT temperature ($\leq$125 °C), whereas it was 0.13 mmol/L for sample S10H155 (Table S3). The total N concentration in the hydrochars decreased with increasing HT temperature as compared to S10 solids (Figure 2c). It was due to the degradation and hydrolysis of organic N into liquid phase,[54] which accordingly resulted in the increasing concentration of NH_4^+ in the HT process water (Table S3). For instance, the total N concentration in solid samples decreased from 3.84 (S10) to 3.29 (S10H155) mmol/g, whereas the NH_4^+ concentration in the HT process water increased from 23.5 (S10) to 62.8 (S10H155) mmol/L.

The AD process enriched metals and total P in the AD solids as compared to their corresponding S10 solids or hydrochars (Figure 1 and Table S2). Mg concentration in the AD process water increased significantly at 10 d in comparison to that in the corresponding S10 supernatant, then decreased with time (Table S3). For instance, Mg concentrations in S10 supernatant and process water samples S10A10, S10A20, and S10A30 are 0.14, 5.94, 2.04, 1.44 mmol/L, respectively. A similar trend is observed for the NH_4^+ concentration. The concentration of Al in AD process water is similar to that in S10 supernatant and HT process water. The concentrations of Ca and PO_4^{3-} in AD process water are lower than those in their corresponding samples S10, S10H90, and S10H125, whereas sample S10H155 released much Ca, Fe, and PO_4^{3-} into the AD process water (Table S3).

For HT-AD with 20 d SRT system, the concentrations of Mg, Fe, Al, Ca, P, and N in S20 solids were 0.46, 0.42, 0.14, 0.45, 0.41, and 3.52 mmol/g (Figure 1 and Table S2), respectively, indicating different elemental composition from S10 solids. Similar trends were observed for the concentrations of Mg, Ca, P, and N in HT hydrochars and AD solids as those in HT-AD with 10 d SRT system (Figure 1 and Table S2). Both HT and AD induced little changes of Al concentration but enriched Fe in the hydrochars and AD solids. For HT process water (Table S3), similar trends are observed for the changes of concentrations of metals, PO_4^{3-}, and NH_4^+ as shown in HT-AD with 10 d SRT system. For AD process water (Table S3), AD increased the concentrations of Mg, Fe, Ca, and NH_4^+ over time as compared to S20 supernatant or the corresponding HT process water. All these metal concen-

trations are much higher than those in HT-AD with 10 d SRT system, due to the different raw sludge matrix and longer SRT. However, similar trends are observed for the changes of Al and PO_4^{3-} concentrations as in HT-AD with 10 d SRT system.

Extracted P and NH_4^+. To evaluate the mobility of P and NH_4^+ in the solid samples, chemical extraction was conducted on raw sludges, HT hydrochars, and AD solids. Figures 2 and S2 show the concentrations and relative abundances of extracted P and NH_4^+ in the solid samples. For HT-AD with the 10 d SRT system, the concentrations of extracted P and NH_4^+ in sample S10 are 0.05 and 0.14 mmol/g (i.e., 12.8% of total P and 3.7% of total N), respectively. With increasing HT temperature, the extracted P concentration decreased in the hydrochars in comparison to that in sample S10, while the extracted NH_4^+ concentration slightly increased. This suggests that the fractions of insoluble P and soluble/exchangeable N in the hydrochars increased with increasing HT temperature. For instance, the concentrations of extracted P and NH_4^+ in sample S10H155 are 0.03 and 0.18 mmol/g (4.6% of total P and 5.3% of total N), respectively. For the AD solids, the extracted concentrations of P and NH_4^+ increased as compared to S10 solids or corresponding hydrochars. In addition, their concentrations decreased with increasing AD time. For instance, the concentrations of extracted P and NH_4^+ are 0.22 mmol/g (20.4% of total P) and 0.29 mmol/g (8.8% of total N) in sample S10H155A10, and 0.16 mmol/g (16.0% of total P) and 0.24 mmol/g (7.1% of total N) for sample S10H155A30, respectively.

In comparison with HT-AD with the 10 d SRT system, similar trends were observed for extracted P and NH_4^+ concentrations in the solid samples from HT-AD with 20 d SRT system (Figure 2). Note that the extracted P and NH_4^+ contents in the two systems were different, due to the different raw sludge matrix.

HT favors the stabilization of P in the hydrochars via the formation of metal phosphate minerals (i.e., Fe, Ca, Mg, or Al associated phosphate),[38] resulting in decreased P bioavailability. However, AD can cause P release, due to microbial dissolution of metal-phosphate minerals and hydrolysis of adenosine triphosphate (ATP) stored in phosphate accumulating organisms (PAOs).[55−59] Both HT and AD favor NH_4^+ release through the degradation and/or hydrolysis of organic N, primarily proteins.

XRD Analysis. To investigate the evolution of mineral phases during HT-AD, XRD analysis was performed on the solid samples. The XRD patterns of the raw sludges, HT hydrochars, and AD solids are shown in Figure 3. For HT-AD with 10 d SRT system (Figure 3a−d), no major crystalline phases were detected for samples S10 and HT hydrochars. The characteristic peaks of struvite are observed for the AD solids from samples S10, S10H90, and S10H125. No struvite peaks are observed in the AD solids from S10H155, suggesting that HT at 155 °C inhibited the formation of struvite in the subsequent AD.

For HT-AD with 20 d SRT system (Figure 3e−h), sample S20 does not show strong diffraction peaks. Vivianite is observed in HT hydrochar samples S20H90 and S20H125, whereas it is absent in sample S20H155. For AD solids, stronger peaks of vivianite are observed in comparison to those in their corresponding S20 solids or HT hydrochars (i.e., S20, S20H90, S20H125, or S20H155), suggesting more vivianite formation in the AD solids. These observations are consistent with our recent study on the formation of vivianite during HT-

Table 2a. Relative Abundance of Different P Species Determined from Linear Combination Fitting (LCF) of P K-Edge XANES Data of the Solid Samples Derived from HT-AD with 10 d SRT System

Sample	Relative abundance (%)										R-factor
	PhyAc	struvite	MgHPO$_4$	Mg$_3$(PO$_4$)$_2$	P–Al$_2$O$_3$	AlPO$_4$	brushite	HAP	ACP	OCP	
S10	13.5 (7.8)		19.2 (6.3)	19.3 (9.2)	18.5 (8.6)		21.1 (9.0)		8.4 (6.7)		0.0057
S10A10		26.8 (3.9)	17.2 (8.4)	10.6 (6.5)	10.7 (6.1)		18.0 (6.4)		9.8 (9.2)	6.9 (9.2)	0.0043
S10A20		18.6 (5.5)		17.8 (9.2)	23.5 (8.6)		12.5 (9.0)	7.0 (8.1)	9.4 (6.3)	11.2 (9.0)	0.0057
S10A30		18.8 (5.3)		18.4 (9.0)	23.7 (8.3)		11.4 (8.8)	7.8 (10.4)	9.1 (5.1)	10.8 (8.0)	0.0052
S10H90	7.6 (9.7)		6.0 (8.0)	20.1 (10.2)	24.4 (9.4)		14.8 (10.1)	7.3 (4.6)	9.9 (3.9)	9.9 (3.4)	0.0061
S10H90A10		21.1 (3.9)	7.4 (6.2)	13.8 (6.5)	22.3 (6.1)		14.6 (6.4)		11.5 (9.0)	9.3 (9.0)	0.0030
S10H90A20		22.7 (4.1)	9.9 (9.1)	15.8 (6.8)	19.4 (6.4)		15.8 (6.7)		9.3 (5.5)	7.1 (9.5)	0.0037
S10H90A30		21.8 (3.5)	17.1 (9.7)	12.5 (5.9)	14.1 (5.5)		16.9 (5.9)		11.4 (10.0)	6.2 (8.2)	0.0028
S10H125				48.2 (9.2)			23.2 (10.0)	10.5 (5.0)	6.2 (6.9)	11.9 (8.9)	0.0078
S10H125A10		15.1 (3.2)	7.3 (8.5)	19.2 (5.3)	22.9 (5.0)		16.2 (5.2)		9.5 (9.0)	9.8 (7.4)	0.0018
S10H125A20		13.6 (3.1)	21.2 (8.7)	9.8 (5.4)	6.4 (5.1)	9.7 (7.8)	19.6 (5.3)		11.9 (9.0)	7.8 (7.5)	0.0024
S10H125A30		15.7 (3.5)	24.4 (9.7)	8.6 (5.9)		11.8 (5.3)	22.0 (5.9)		10.6 (10.0)	6.9 (8.2)	0.0034
S10H155			14.9 (6.9)	44.5 (10.0)			25.2 (7.6)	8.9 (7.3)		6.5 (7.4)	0.0075
S10H155A10			21.1 (8.0)	20.5 (4.9)	19.9 (4.5)		20.0 (4.8)		12.7 (8.1)	5.8 (6.6)	0.0017
S10H155A20			21.3 (8.3)	16.9 (5.0)	23.7 (4.6)		19.3 (5.0)		18.8 (8.4)		0.0016
S10H155A30			22.4 (7.4)	14.1 (4.5)	24.4 (4.1)		17.7 (4.4)		21.4 (7.5)		0.0013

^{a}LCF derived errors (%) are given in parentheses. ^{b}PhyAc, P–Al$_2$O$_3$, HAP, ACP, and OCP are phytic acid, phosphate sorbed on Al$_2$O$_3$, hydroxyapatite, amorphous calcium phosphate, and octacalcium phosphate, respectively.

Table 2b. Relative Abundance of Different P Species Determined from Linear Combination Fitting (LCF) of P K-Edge XANES Data of the Solid Samples Derived from HT-AD with 20 d SRT System

Sample	Relative abundance (%)									R-factor
	PhyAc	vivianite	strengite	P-Ferrihy	$Mg_3(PO_4)_2$	$AlPO_4$	HAP	ACP	OCP	
S20	19.8 (7.1)			8.1 (5.4)	17.4 (6.9)	7.8 (7.3)	11.9 (5.1)	20.1 (10.0)	14.9 (8.9)	0.0108
S20A32		41.1 (2.6)		13.3 (4.7)	22.6 (2.2)			16.0 (4.4)	7.0 (3.7)	0.0008
S20A62		31.1 (5.6)		19.0 (10.5)	29.6 (5.0)			10.8 (9.7)	9.5 (8.2)	0.0030
S20H90	13.4 (11.6)	25.4 (5.6)		9.4 (9.2)	17.3 (4.2)		8.2 (9.2)	15.0 (7.5)	11.3 (6.6)	0.0045
S20H90A32		37.2 (2.6)		13.2 (4.9)	32.3 (2.2)			10.1 (4.5)	7.2 (3.7)	0.0007
S20H90A62		60.0 (2.3)			20.2 (2.1)			19.8 (4.1)		0.0007
S20H125		22.1 (5.8)		10.3 (9.3)	23.6 (5.1)		12.2 (10.2)	16.9 (10.4)	14.9 (7.6)	0.0053
S20H125A32		46.4 (2.8)			23.2 (2.5)	10.6 (2.7)		19.8 (5.0)		0.0010
S20H125A62		27.4 (2.8)		22.2 (5.1)	35.4 (2.4)			8.2 (4.7)	6.8 (4.1)	0.0007
S20H155			18.2 (1.0)		47.7 (1.3)			23.8 (3.5)	10.3 (5.4)	0.0023
S20H155A32		19.1 (2.9)	11.0 (1.0)		46.4 (0.8)		8.7 (4.7)	8.1 (4.8)	6.7 (4.3)	0.0008
S20H155A62		6.0 (3.6)	22.2 (1.2)		44.4 (0.9)		11.0 (5.7)	6.2 (5.9)	10.2 (5.2)	0.0010

[a]LCF derived errors (%) are given in parentheses. [b]PhyAc, P-Ferrihy, HAP, ACP, and OCP are phytic acid, phosphate sorbed on ferrihydrite, hydroxyapatite, amorphous calcium phosphate, and octacalcium phosphate, respectively.

AD using batch AD assays.[34] Note that the broad hump at 15–25° 2θ of the XRD spectra of the solid samples is observed, due to presence of amorphous lignin and cellulose in sewage sludge.[60,61]

P K-Edge XANES Spectroscopy. To quantify the speciation of P in the solid samples, P XANES LCF analysis was conducted using the standard compounds listed in Figure S2 and the best fitting results are presented in Table 2 and Figure S3. For HT-AD with 10 d SRT system (Table 2a), phyAc (13.5%), $MgHPO_4$ (19.2%), $Mg_3(PO_4)_2$ (19.3%), P–Al_2O_3 (18.5%), brushite (21.1%), and ACP (8.4%) are the main P species in sample S10. PhyAc is absent in HT hydrochars and AD solids except for sample S10H90 (7.6%), suggesting that HT at 125 and 155 °C and AD induced the complete transformation of organic P to inorganic P through decomposition and hydrolysis. In comparison with those of sample S10, the fractions of PhyAc and P–Al_2O_3 decreased in HT hydrochars, whereas the fractions of Mg-associated P and Ca-associated P increased. Such changes become more significant with increasing HT temperature. These results suggest that HT produced inorganic P formed insoluble Ca/Mg–P minerals. For instance, the fractions of Mg-associated P and Ca-associated P in sample S10H155 reached 59.4% and 40.6%, respectively, much higher than those in sample S10. For AD solids of S10 alone (without HT), the fractions of phyAc and Mg-associated P in samples S10A10, S10A20, and S10A30 decreased in comparison to those in sample S10, while the fractions of struvite and Ca-associated P increased. The fraction of struvite in these AD solids was 18.6–26.8%. The fraction of Al-associated P in these AD solids did not change significantly in comparison to that in sample S10. For AD of S10H90 slurries, struvite fraction in AD solids increased to 21.1–22.7% in comparison to that in sample S10H90, while the fractions of phyAc and Mg/Al-associated P decreased. The change of Ca-associated P fractions is within <10%. The conversion of $Mg_3(PO_4)_2$ into struvite, $MgHPO_4$, and/or P–Al_2O_3 was observed during AD of S10H125, and the fraction of struvite in AD solids S10H125A10, S10H125A20, and S10H125A30 is 13.6–15.7%. No struvite was observed in samples S10H155A10, S10H155A20, and S10H155A30, but partial conversion of $Mg_3(PO_4)_2$ into P–Al_2O_3 was observed. The fraction of P–Al_2O_3 in these AD solids is 19.9–24.4%.

For HT-AD with the 20 d SRT system, inclusion of Fe-associated P minerals (vivianite, strengite, P-ferrihydrite) yielding best fitting results for LCF analysis, as the concentration of Fe in solid sample S20 was much higher that of sample S10. LCF analyses identified phyAc (19.8%), P-ferrihydrite (8.1%), $Mg_3(PO_4)_2$ (17.4%), $AlPO_4$ (7.8%), HAP (11.9%), ACP (20.1%), and OCP (14.9%) as the main P species in sample S20 (Table 2b). For HT hydrochars and AD solids, phyAc (13.4%) is only present in sample S20H90, consistent with the results of HT-AD with 10 d SRT system. The fractions of P-ferrihydrite, $Mg_3(PO_4)_2$, HAP, ACP, and OCP in samples S20H90 and S20H125 changed within 10% as compared to sample S20, whereas the fraction of vivianite increased from 0 (S20) to 25.4% and 22.1% (S20H90 and S20H125). No vivianite was fitted for sample S20H155, while the fractions of strengite and ACP increased from 0 and 20.1% (S20) to 24.6% and 54.2% (S20H155). For the subsequent AD, the fraction of vivianite in the AD solids increased in comparison to those in their corresponding raw sludge or HT hydrochar samples, although vivianite fraction fluctuated with different AD time. In addition, the fraction of vivianite in the AD solids derived from samples S20H90 and S20H125 was higher than that in AD solids derived from sample S20H155. For instance, vivianite fractions in samples S20H90A62, S20H125A62, and S20H155A62 are 60.0%, 27.4%, and 6.0%, respectively.

XAS analysis (including LCF analysis) is an *in situ*, nondestructive, and highly sensitive method, providing molecular-scale information and tracing the chemical environments of a specific element. Typical fitting errors for LCF of XAS data is ~10%, due to the difficulty in establishing a complete library of standard compounds for such complex and heterogeneous matrix (sludge) and potential spectra similarities for some standard compounds. Note that our LCF analysis results mainly reflected the trends of P speciation change in sludge during HT-AD.

XPS Spectroscopy. To investigate the speciation evolution of N in the solid samples during HT-AD, the N-containing functional groups in raw sludges, HT hydrochars, and AD solids were characterized by N 1s XPS spectra (Figures S4 and S5). For HT-AD with the 10 d SRT system (Figure S4), in comparison to that in sample S10, the main peak position of HT hydrochar samples shifted slightly to high binding energy
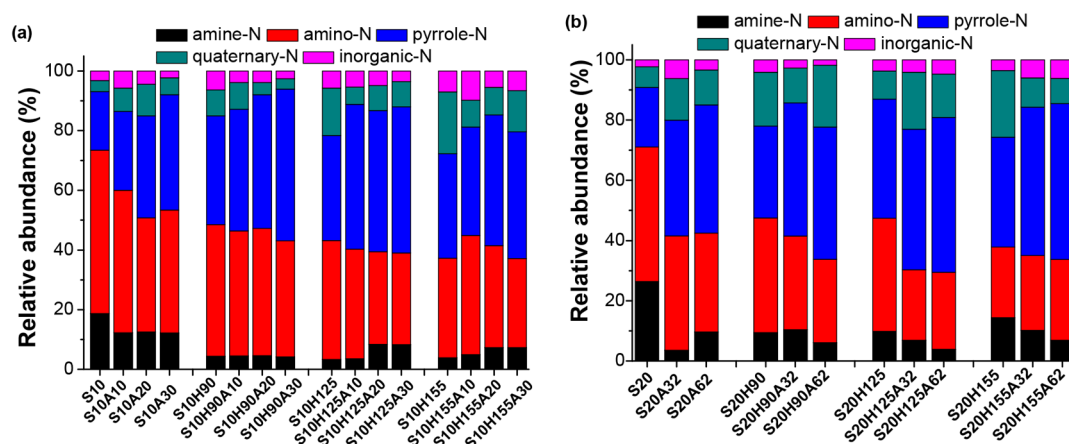
Figure 4. Relative abundance of different N species in the solid samples determined from deconvolution of N 1s XPS spectra. (a) HT-AD with 10 d SRT system; (b) HT-AD with 20 d SRT system.

with increasing HT temperature (Figure S4a). Similar trends were observed for the AD solids as those of their corresponding raw sludge or HT hydrochars. However, such shifting became weaker for the AD solids from high temperature HT. Similar trends were observed in HT-AD with 20 d SRT system (Figure S5). For instance, the XPS spectra of S20H155 and S20H155A32 were similar, suggesting that AD of S20H155 slurries did not induce significant N fraction change.

Spectral deconvolution of solid samples in HT-AD with the 10 d SRT system is shown in Figures S6 and 4a. Sample S10 is dominated by amine- and amino-N (~71%), followed by pyrrole-N (10%), quaternary-N (2%), and inorganic-N (2%). The fraction of amine- and amino-N in HT hydrochars decreased with increasing HT temperature as compared to sample S10, while the fraction of pyrrole- and quaternary-N significantly increased. The change of inorganic N fraction fluctuated within 5%. For instance, the fractions of amine-, amino-, pyrrole-, quaternary-, and inorganic-N in sample S10H155 are 2%, 30%, 30%, 15%, and 5%, respectively. For the subsequent AD alone, the fraction of amine- and amino-N in samples S10A10, S10A20, and S10A30 decreased in comparison to that in sample S10, while the fraction of pyrrole-N increased. For instance, the fractions of amine-, amino-, pyrrole-, quaternary-, and inorganic-N in sample S10A30 are 12%, 30%, 38%, 4%, and 1%, respectively. In comparison with that in HT hydrochars, quaternary-N fraction in the subsequent AD solids decreased while pyrrole-N fraction increased. For instance, the fractions of amine-, amino-, pyrrole-, quaternary-, and inorganic-N in sample S10H155A30 are 8%, 32%, 44%, 8%, and 4%, respectively. The fraction of each N speciation in AD solids collected at different times did not change significantly (within 5%).

For HT-AD 20 d with SRT system (Figures S7 and 4b), the N speciation in sample S20 is similar to that in sample S10. The speciation evolution trends of N during HT and AD processes are similar to those in HT-AD with 10 d SRT system. Note that the XPS fitting analysis mainly reflected the change trends of each N fraction during HT-AD.

Transformation of N during HT-AD. During HT, amino-N functional groups are hydrolyzed into NH_4^+,[62] resulting in a high concentration of NH_4^+ in HT process water. A higher concentration of NH_4^+ is observed in the HT process water derived from higher temperatures, likely due to the increased

hydrolysis rate. Zhuang et al.[54] also reported that amino-N can be converted into quaternary-N by polymerization and ring condensation during HT of biomass. The increased content of pyrrole-N (a type of heterocyclic-N) in hydrochars is caused by cyclization and ring condensation of N intermediates via Diels−Alder reaction.[63,64] High HT temperature favors this reaction. In addition, amine-N can be converted into other N functionalities (no amino-N) along with the release of ammonium N at high temperature.[2] It should be noted that few N gas compounds can be produced during HT of sludge below 180 °C.[54]

During AD, degradation of amine- and amnio-N compounds can release NH_4^+.[65,66] Quaternary-N compounds can be transformed into amines via anaerobic fermentation,[67] followed by degradation to generate NH_4^+. However, pyrrole-N compounds are resistant to anaerobic microbial processes due to their stable structures, resulting in the accumulation of pyrrole-N in the AD solids.

Formation of Struvite Vs Vivianite during HT-AD. Struvite precipitation can occur in a wide pH range (7−11) following eq 1:[68]

$$Mg^{2+} + NH_4^+ + H_nPO_4^{n-3} + 6H_2O$$
$$\rightarrow MgNH_4PO_4 \cdot 6H_2O + nH^+ \qquad (1)$$
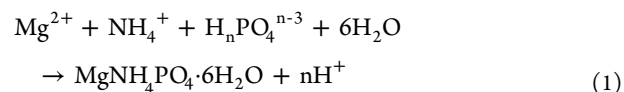
The crystallization rate is strongly dependent on pH. Low pH significantly reduces the rate of crystallization and enhances the solubility of struvite,[69,70] whereas high pH causes the evaporation of NH_3. Thus, the most suitable pH range for struvite precipitation is 7.5−9. For HT-AD with 10 d SRT system, the pH values of HT slurries at 90, 125, 155 °C are below 7 (Table 1), thus not favorable for struvite precipitation in HT hydrochars (i.e., samples S10H90, S10H125, and S10H155). However, the coexistence of abundant Mg and phosphate induced the formation of amorphous $Mg_3(PO_4)_2/MgHPO_4$ in the hydrochars. For sludge treated with AD alone (not HT), struvite is precipitated in samples S10A10, S10A20, and S10A30, due to the coexistence of Mg^{2+}, PO_4^{3-} and NH_4^+ at pH ~ 7.4 (Tables 1, S2, and S3). The soluble Mg^{2+}, PO_4^{3-}, and NH_4^+ resulted from microbial dissolution of Mg phosphate minerals, desorption from other minerals, and/or degradation of organic N. However, the amount of struvite in these AD solids is not high, consistent with previous observations that struvite precipitation from an AD supernatant at pH 7−8 was

very slow and took several days.[32,71] In addition, the presence of Ca and/or Fe (Tables S2 and S3) inhibited struvite crystal growth and decreased struvite purity.[72,73] For the subsequent AD of S10H90 and S10H125 slurries (pH ~ 7.3 (Table 1)), struvite was precipitated in the AD solids as described by the following equation:[74]

$$Mg_3(PO_4)_2 + 2NH_3 + 14H_2O$$

$$\rightarrow 2MgNH_4PO_4 \cdot 6H_2O + Mg(OH)_2 \qquad (2)$$
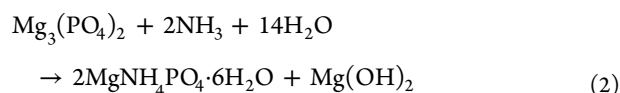
Bhuiyan et al.[75] also reported that amorphous $MgHPO_4$ can transform into struvite in the presence of NH_4^+. NH_4^+ was from the decomposition and hydrolysis of organic N during both HT and AD. The extensive NH_4^+ in the subsequent AD process did not induce transformation of all $Mg_3(PO_4)_2$/$MgHPO_4$ into struvite, as the pH (7.32−7.48) was not high enough (Table 1). Struvite did not form during AD of S10H155 slurries, as the pH was at ~7 during the whole process (Table 1).

For HT-AD with the 20 d SRT system (pH range 7.24−7.74 for all conditions), struvite is not observed in the HT hydrochars and AD solids, due to the high molar ratio of Fe/Mg (1:1.1) and the stronger affinity of Fe than Mg toward P.[73] The inhibition effect of Ca is previously observed, but its effect is much weaker than Fe.[73] Considering that Ca content was high (i.e., the molar ratio of Ca/Mg is 1) in sample S20 (Table S2), presence of Ca may have also contributed to the inhibition of struvite precipitation in AD. However, the molar ratios of Fe/Mg and Ca/Mg in sample S10 are 0.17 and 0.37 (Table S2), respectively, much lower than those in sample S20. Thus, precipitation of struvite was able to occur in HT-AD with 10 d SRT system at pH > 7.

Regarding the formation of vivianite during HT-AD with the 20 d SRT system using sewage sludge rich in Fe and P, the reaction pathways are similar to those that occurred in batch AD assays reported in our recent study.[34,49] Briefly, intermediates such as 5-hydroxymethylfurfural (5-HMF) generated during HT hydrolysis of cellulose in sewage sludge at HT low temperature (i.e., 90 and 125 °C) can reduce Fe(III) species into Fe(II), which preferentially precipitates with P to form vivianite. However, 5-HMF can further form hydrochars via polymerization and condensation at HT high temperature (i.e., 155 °C), which cannot easily reduce the Fe(III) species. For the AD process, microbial reduction of Fe(III) species makes soluble Fe(II) available which reacts with soluble P quickly to form vivianite.

The differences in SRTs did not affect the formation of struvite or vivianite during HT-AD. The formation of struvite or vivianite during HT-AD was mainly influenced by the molar ratios of Fe:Mg. For instance, our batch-scale research[34] of HT-AD using a Fe:Mg molar ratio of 1:1.2 reported similar results as that of T-AD with 20 d SRT (molar ratio of Fe: Mg = 1:1.1). Moreover, the purpose of this study is to assess the formation of struvite or vivianite during HT-AD with different SRTs.

CONCLUSIONS

The formation of struvite vs vivianite and the transformation of N in sewage sludge during semicontinuous AD with prestage HT were studied using complementary chemical extraction and X-ray based methods. Here are the main results: (1) The precipitation of struvite in HT hydrochars and AD solids is highly dependent on pH and Mg/Fe molar ratio. (2) Struvite can form via the reaction between $Mg_3(PO_4)_2$/$MgHPO_4$ and NH_4^+ at pH > 7 during AD. (3) HT at low temperature (90 and 125 °C) favors the formation of vivianite in the hydrochars, while HT at high temperature (155 °C) favors the formation of strengite. AD of HT slurries can further reduce Fe(III) species to Fe(II) and form vivianite. (4) HT induces the accumulation of quaternary- and pyrrole-N in the hydrochars while only pyrrole-N is enriched in the AD solids. HT and AD degrade other organic N species to generate large amounts of NH_4^+ in HT and AD process waters. Considering that 55% of sewage sludge is land applied in United States,[29] the speciation information on P and N in this study provides fundamental knowledge on hydrochars and AD solids derived from HT-AD serving as fertilizers. For instance, Blue Plains Advanced Wastewater Treatment Plant in Washington, DC, in the United States, has adopted a HT-AD process that produces Class A biosolids for land application in addition to production of biomethane. This study also provides insights for nutrient recovery from the final AD solids. For instance, vivianite formed in the anaerobically digested sludge can be recovered via microbial electrolysis cell[25] or magnetic separation.[20] The conditions of prestage HT of sludge rich in Mg and P can predict the precipitation of struvite in the subsequent AD. Moreover, the findings shed light on the selection and optimization of struvite precipitation. For instance, the high production of struvite in subsequent AD might be achieved by adjusting the pH of the HT slurries to an alkaline condition.[68] Anaerobically digested sludge rich in struvite can serve as a slow-release P and N fertilizer.

ASSOCIATED CONTENT

Supporting Information

The Supporting Information is available free of charge at https://pubs.acs.org/doi/10.1021/acssuschemeng.1c02638.

P standard compounds for P K-edge XANES analysis; analysis of the major metal concentrations, total P, and total N in the solids; analysis of the major metal concentrations, PO_4^{3-}, and NH_4^+ in process waters; analysis of extracted P and NH_4^+ in the solids; results of P K-edge XANES analysis; and results of N 1s XPS analysis (PDF)

AUTHOR INFORMATION

Corresponding Author

Yuanzhi Tang − *School of Earth and Atmospheric Sciences,, Georgia Institute of Technology, Atlanta, Georgia 30332-0340, United States; School of Civil and Environmental Engineering, Georgia Institute of Technology, Atlanta, Georgia 30332-0512, United States;* ⓘ orcid.org/0000-0002-7741-8646; Phone: (1) 404-894-3814; Email: yuanzhi.tang@eas.gatech.edu

Authors

Qian Wang − *School of Earth and Atmospheric Sciences,, Georgia Institute of Technology, Atlanta, Georgia 30332-0340, United States*

Xiaoguang Liu − *School of Civil and Environmental Engineering, Georgia Institute of Technology, Atlanta, Georgia 30332-0512, United States*

Haesung Jung − *School of Earth and Atmospheric Sciences,, Georgia Institute of Technology, Atlanta, Georgia 30332-*

0340, United States; School of Civil, Environmental and Chemical Engineering, Changwon National University, Changwon, Gyeongsangnam-do 51140, Republic of Korea; orcid.org/0000-0002-8795-248X

Simin Zhao − School of Earth and Atmospheric Sciences,, Georgia Institute of Technology, Atlanta, Georgia 30332-0340, United States

Spyros G. Pavlostathis − School of Civil and Environmental Engineering, Georgia Institute of Technology, Atlanta, Georgia 30332-0512, United States; orcid.org/0000-0001-9731-3836

Complete contact information is available at:
https://pubs.acs.org/10.1021/acssuschemeng.1c02638

Notes

The authors declare no competing financial interest.

REFERENCES

(1) Martí, N.; Pastor, L.; Bouzas, A.; Ferrer, J.; Seco, A. Phosphorus recovery by struvite crystallization in WWTPs: Influence of the sludge treatment line operation. *Water Res.* **2010**, *44* (7), 2371−2379.

(2) Tian, K.; Liu, W.-J.; Qian, T.-T.; Jiang, H.; Yu, H.-Q. Investigation on the evolution of N-containing organic compounds during pyrolysis of sewage sludge. *Environ. Sci. Environ. Sci. Technol.* **2014**, *48* (18), 10888−10896.

(3) Huang, R.; Tang, Y. Evolution of phosphorus complexation and mineralogy during (hydro)thermal treatments of activated and anaerobically digested sludge: Insights from sequential extraction and P K-edge XANES. *Water Res.* **2016**, *100*, 439−447.

(4) He, C.; Wang, K.; Yang, Y.; Amaniampong, P. N.; Wang, J.-Y. Effective nitrogen removal and recovery from dewatered sewage sludge using a novel integrated system of accelerated hydrothermal deamination and air stripping. *Environ. Sci. Technol.* **2015**, *49* (11), 6872−6880.

(5) Xie, M.; Nghiem, L. D.; Price, W. E.; Elimelech, M. Toward resource recovery from wastewater: extraction of phosphorus from digested sludge using a hybrid forward osmosis−membrane distillation process. *Environ. Sci. Technol. Lett.* **2014**, *1* (2), 191−195.

(6) Ortega-Martinez, E.; Sapkaite, I.; Fdz-Polanco, F.; Donoso-Bravo, A. From pre-treatment toward inter-treatment. Getting some clues from sewage sludge biomethanation. *Bioresour. Technol.* **2016**, *212*, 227−235.

(7) Liu, X.; Wang, Q.; Tang, Y.; Pavlostathis, S. G. A comparative study on biogas production, energy balance, and nutrients conversion with inter-stage hydrothermal treatment of sewage sludge. *Appl. Energy* **2021**, *288*, 116669.

(8) Huang, R.; Zhang, B.; Saad, E. M.; Ingall, E. D.; Tang, Y. Speciation evolution of zinc and copper during pyrolysis and hydrothermal carbonization treatments of sewage sludges. *Water Res.* **2018**, *132*, 260−269.

(9) Westerhoff, P.; Lee, S.; Yang, Y.; Gordon, G. W.; Hristovski, K.; Halden, R. U.; Herckes, P. Characterization, recovery opportunities, and valuation of metals in municipal sludges from U.S. wastewater treatment plants nationwide. *Environ. Sci. Technol.* **2015**, *49* (16), 9479−9488.

(10) Wang, Q.; Zhang, C.; Jung, H.; Liu, P.; Patel, D.; Pavlostathis, S. G.; Tang, Y. Transformation and mobility of Cu, Zn, and Cr in sewage sludge during anaerobic digestion with pre- or interstage hydrothermal treatment. *Environ. Sci. Technol.* **2021**, *55* (3), 1615−1625.

(11) McCarty, P. L.; Bae, J.; Kim, J. Domestic wastewater treatment as a net energy producer−can this be achieved? *Environ. Sci. Technol.* **2011**, *45* (17), 7100−7106.

(12) Choi, J.-M.; Han, S.-K.; Lee, C.-Y. Enhancement of methane production in anaerobic digestion of sewage sludge by thermal hydrolysis pretreatment. *Bioresour. Technol.* **2018**, *259*, 207−213.

(13) Kor-Bicakci, G.; Eskicioglu, C. Recent developments on thermal municipal sludge pretreatment technologies for enhanced anaerobic digestion. *Renewable Sustainable Energy Rev.* **2019**, *110*, 423−443.

(14) Pavlostathis, S. G. 6.31. Kinetics and modeling of anaerobic treatment and biotransformation processes. *Comprehensive Biotechnology* **2011**, *6*, 385−397.

(15) Vavilin, V. A.; Fernandez, B.; Palatsi, J.; Flotats, X. Hydrolysis kinetics in anaerobic degradation of particulate organic material: An overview. *Waste Manage.* **2008**, *28* (6), 939−951.

(16) Fang, C.; Huang, R.; Dykstra, C.; Jiang, R.; Pavlostathis, S. G.; Tang, Y. Energy and nutrient recovery from sewage sludge and manure via anaerobic digestion with hydrothermal pretreatment. *Environ. Sci. Technol.* **2020**, *54* (2), 1147−1156.

(17) Li, C.; Wang, X.; Zhang, G.; Yu, G.; Lin, J.; Wang, Y. Hydrothermal and alkaline hydrothermal pretreatments plus anaerobic digestion of sewage sludge for dewatering and biogas production: Bench-scale research and pilot-scale verification. *Water Res.* **2017**, *117*, 49−57.

(18) Qiao, W.; Yan, X.; Ye, J.; Sun, Y.; Wang, W.; Zhang, Z. Evaluation of biogas production from different biomass wastes with/without hydrothermal pretreatment. *Renewable Energy* **2011**, *36* (12), 3313−3318.

(19) Passos, F.; Ferrer, I. Influence of hydrothermal pretreatment on microalgal biomass anaerobic digestion and bioenergy production. *Water Res.* **2015**, *68*, 364−373.

(20) Prot, T.; Nguyen, V. H.; Wilfert, P.; Dugulan, A. I.; Goubitz, K.; De Ridder, D. J.; Korving, L.; Rem, P.; Bouderbala, A.; Witkamp, G. J.; van Loosdrecht, M. C. M. Magnetic separation and characterization of vivianite from digested sewage sludge. *Sep. Purif. Technol.* **2019**, *224*, 564−579.

(21) Prot, T.; Wijdeveld, W.; Eshun, L. E.; Dugulan, A. I.; Goubitz, K.; Korving, L.; Van Loosdrecht, M. C. M. Full-scale increased iron dosage to stimulate the formation of vivianite and its recovery from digested sewage sludge. *Water Res.* **2020**, *182*, 115911.

(22) Wilfert, P.; Dugulan, A. I.; Goubitz, K.; Korving, L.; Witkamp, G. J.; Van Loosdrecht, M. C. M. Vivianite as the main phosphate mineral in digested sewage sludge and its role for phosphate recovery. *Water Res.* **2018**, *144*, 312−321.

(23) Wilfert, P.; Mandalidis, A.; Dugulan, A. I.; Goubitz, K.; Korving, L.; Temmink, H.; Witkamp, G. J.; Van Loosdrecht, M. C. M. Vivianite as an important iron phosphate precipitate in sewage treatment plants. *Water Res.* **2016**, *104*, 449−460.

(24) Wu, H.; Ikeda-Ohno, A.; Wang, Y.; Waite, T. D. Iron and phosphorus speciation in Fe-conditioned membrane bioreactor activated sludge. *Water Res.* **2015**, *76*, 213−226.

(25) Wilfert, P.; Kumar, P. S.; Korving, L.; Witkamp, G.-J.; van Loosdrecht, M. C. M. The relevance of phosphorus and iron chemistry to the recovery of phosphorus from wastewater: A review. *Environ. Sci. Technol.* **2015**, *49* (16), 9400−9414.

(26) Marti, N.; Bouzas, A.; Seco, A.; Ferrer, J. Struvite precipitation assessment in anaerobic digestion processes. *Chem. Eng. J.* **2008**, *141* (1), 67−74.

(27) Ohlinger, K. N.; Young, T. M.; Schroeder, E. D. Predicting struvite formation in digestion. *Water Res.* **1998**, *32* (12), 3607−3614.

(28) Martí, N.; Barat, R.; Seco, A.; Pastor, L.; Bouzas, A. Sludge management modeling to enhance P-recovery as struvite in wastewater treatment plants. *J. Environ. Manage.* **2017**, *196*, 340−346.

(29) Peccia, J.; Westerhoff, P. We should expect more out of our sewage sludge. *Environ. Sci. Technol.* **2015**, *49* (14), 8271−8276.

(30) Plaza, C.; Sanz, R.; Clemente, C.; Fernández, J. M.; González, R.; Polo, A.; Colmenarejo, M. F. Greenhouse evaluation of struvite and sludges from municipal wastewater treatment works as phosphorus sources for plants. *J. Agric. Food Chem.* **2007**, *55* (20), 8206−8212.

(31) Korving, L.; Van Loosdrecht, M.; Wilfert, P., Effect of iron on phosphate recovery from sewage sludge (Book Chapter). In *In: Phosphorus recovery and recycling*; Springer: 2018; pp 303−326. DOI: 10.1007/978-981-10-8031-9_21.

(32) Battistoni, P.; Fava, G.; Pavan, P.; Musacco, A.; Cecchi, F. Phosphate removal in anaerobic liquors by struvite crystallization without addition of chemicals: Preliminary results. *Water Res.* **1997**, *31* (11), 2925−2929.

(33) Marti, N.; Ferrer, J.; Seco, A.; Bouzas, A. Optimisation of sludge line management to enhance phosphorus recovery in WWTP. *Water Res.* **2008**, *42* (18), 4609−4618.

(34) Wang, Q.; Zhang, C.; Patel, D.; Jung, H.; Liu, P.; Wan, B.; Pavlostathis, S. G.; Tang, Y. Coevolution of iron, phosphorus, and sulfur speciation during anaerobic digestion with hydrothermal pretreatment of sewage sludge. *Environ. Sci. Technol.* **2020**, *54* (13), 8362−8372.

(35) Liu, J.; Zheng, J.; Zhang, J.; Yu, D.; Wei, Y. The performance evaluation and kinetics response of advanced anaerobic digestion for sewage sludge under different SRT during semi-continuous operation. *Bioresour. Technol.* **2020**, *308*, 123239.

(36) Ghanim, B. M.; Kwapinski, W.; Leahy, J. J. Speciation of nutrients in hydrochar produced from hydrothermal carbonization of poultry litter under different treatment conditions. *ACS Sustainable Chem. Eng.* **2018**, *6* (9), 11265−11272.

(37) Heilmann, S. M.; Molde, J. S.; Timler, J. G.; Wood, B. M.; Mikula, A. L.; Vozhdayev, G. V.; Colosky, E. C.; Spokas, K. A.; Valentas, K. J. Phosphorus reclamation through hydrothermal carbonization of animal manures. *Environ. Sci. Technol.* **2014**, *48* (17), 10323−10329.

(38) Huang, R.; Tang, Y. Speciation dynamics of phosphorus during (hydro)thermal treatments of sewage sudge. *Environ. Sci. Environ. Sci. Technol.* **2015**, *49* (24), 14466−14474.

(39) Frost, R. L.; Weier, M. L.; Erickson, K. L. Thermal decomposition of struvite. *J. Therm. Anal. Calorim.* **2004**, *76* (3), 1025−1033.

(40) Tansel, B.; Lunn, G.; Monje, O. Struvite formation and decomposition characteristics for ammonia and phosphorus recovery: A review of magnesium-ammonia-phosphate interactions. *Chemosphere* **2018**, *194*, 504−514.

(41) Bayuseno, A. P.; Schmahl, W. W. Hydrothermal synthesis of struvite and its phase transition: Impacts of pH, heating and subsequent cooling methods. *J. Cryst. Growth* **2018**, *498*, 336−345.

(42) Sarwar, R.; Elbeshbishy, E.; Parker, W. J. Codigestion of high pressure thermal hydrolysis-treated thickened waste activated sludge with primary sludge in two-stage anaerobic digestion. *Environ. Prog. Sustainable Energy* **2018**, *37* (1), 425−433.

(43) Liu, X.; Wang, Q.; Tang, Y.; Pavlostathis, S. G. Hydrothermal pretreatment of sewage sludge for enhanced anaerobic digestion: Resource transformation and energy balance. *Chem. Eng. J.* **2021**, *410*, 127430.

(44) Zhang, C.; Liu, X.; Wang, Q.; Tang, Y.; Pavlostathis, S. G., Comparative assessment of pre- and inter-stage hydrothermal treatment of municipal sludge for increased methane production. *Water Environ. Res.* **2021**, in press. DOI: 10.1002/wer.1523.

(45) Kahiluoto, H.; Kuisma, M.; Ketoja, E.; Salo, T.; Heikkinen, J. Phosphorus in manure and sewage sludge more recyclable than in soluble inorganic fertilizer. *Environ. Sci. Technol.* **2015**, *49* (4), 2115−2122.

(46) Olsen, S. R. *Estimation of available phosphorus in soils by extraction with sodium bicarbonate.* US Department of Agriculture: 1954. https://www.semanticscholar.org/paper/Estimation-of-available-phosphorus-in-soils-by-with-Olsen/681a42d80a5dd02d2917a7ec4af079916c576f29#paper-header.

(47) Dorich, R. A.; Nelson, D. W. Direct colorimetric measurement of ammonium in potassium chloride extracts of soils. *Soil Sci. Soc. Am. J.* **1983**, *47* (4), 833−836.

(48) Ravel, B.; Newville, M. ATHENA, ARTEMIS, HEPHAESTUS: data analysis for X-ray absorption spectroscopy using IFEFFIT. *J. Synchrotron Radiat.* **2005**, *12* (4), 537−541.

(49) Wang, Q.; Zhang, C.; Liu, P.; Jung, H.; Wan, B.; Patel, D.; Pavlostathis, S. G.; Tang, Y. Effect of inter-stage hydrothermal treatment on anaerobic digestion of sewage sludge: Speciation evolution of phosphorus, iron, and sulfur. *ACS Sustainable Chem. Eng.* **2020**, *8* (44), 16515−16525.

(50) Meng, X.; Wang, Q.; Wan, B.; Xu, J.; Huang, Q.; Yan, J.; Tang, Y. Transformation of phosphorus during low-temperature co-combustion of sewage sludge with biowastes. *ACS Sustainable Chem. Eng.* **2021**, *9* (10), 3668−3676.

(51) Shober, A. L.; Hesterberg, D. L.; Sims, J. T.; Gardner, S. Characterization of phosphorus species in biosolids and manures using XANES spectroscopy. *J. Environ. Qual.* **2006**, *35* (6), 1983−1993.

(52) Kelemen, S. R.; Freund, H.; Gorbaty, M. L.; Kwiatek, P. J. Thermal chemistry of nitrogen in kerogen and low-rank coal. *Energy Fuels* **1999**, *13* (2), 529−538.

(53) Kelemen, S. R.; Gorbaty, M. L.; Kwiatek, P. J. Quantification of nitrogen forms in Argonne Premium coals. *Energy Fuels* **1994**, *8* (4), 896−906.

(54) Zhuang, X.; Huang, Y.; Song, Y.; Zhan, H.; Yin, X.; Wu, C. The transformation pathways of nitrogen in sewage sludge during hydrothermal treatment. *Bioresour. Technol.* **2017**, *245*, 463−470.

(55) Latif, M. A.; Mehta, C. M.; Batstone, D. J. Low pH anaerobic digestion of waste activated sludge for enhanced phosphorous release. *Water Res.* **2015**, *81*, 288−293.

(56) Vardanyan, A.; Kafa, N.; Konstantinidis, V.; Shin, S. G.; Vyrides, I. Phosphorus dissolution from dewatered anaerobic sludge: Effect of pHs, microorganisms, and sequential extraction. *Bioresour. Technol.* **2018**, *249*, 464−472.

(57) Nielsen, P. H.; McIlroy, S. J.; Albertsen, M.; Nierychlo, M. Re-evaluating the microbiology of the enhanced biological phosphorus removal process. *Curr. Opin. Biotechnol.* **2019**, *57*, 111−118.

(58) Latif, M. A.; Mehta, C. M.; Batstone, D. J. Influence of low pH on continuous anaerobic digestion of waste activated sludge. *Water Res.* **2017**, *113*, 42−49.

(59) Latif, M. A.; Mehta, C. M.; Batstone, D. J. Enhancing soluble phosphate concentration in sludge liquor by pressurised anaerobic digestion. *Water Res.* **2018**, *145*, 660−666.

(60) Aliakbari, Z.; Younesi, H.; Ghoreyshi, A. A.; Bahramifar, N.; Heidari, A. Production and characterization of sewage-sludge based activated carbons under different post-activation conditions. *Waste Biomass Valorization* **2018**, *9* (3), 451−463.

(61) Park, S.; Baker, J. O.; Himmel, M. E.; Parilla, P. A.; Johnson, D. K. Cellulose crystallinity index: measurement techniques and their impact on interpreting cellulase performance. *Biotechnol. Biofuels* **2010**, *3* (1), 10.

(62) Kruse, A.; Koch, F.; Stelzl, K.; Wüst, D.; Zeller, M. Fate of nitrogen during hydrothermal carbonization. *Energy Fuels* **2016**, *30* (10), 8037−8042.

(63) Tian, Y.; Zhang, J.; Zuo, W.; Chen, L.; Cui, Y.; Tan, T. Nitrogen conversion in relation to NH3 and HCN during microwave pyrolysis of sewage sludge. *Environ. Sci. Technol.* **2013**, *47* (7), 3498−3505.

(64) Zhang, B.; Xiong, S.; Xiao, B.; Yu, D.; Jia, X. Mechanism of wet sewage sludge pyrolysis in a tubular furnace. *Int. J. Hydrogen Energy* **2011**, *36* (1), 355−363.

(65) Park, J.; Park, S.; Kim, M. Anaerobic degradation of amino acids generated from the hydrolysis of sewage sludge. *Environ. Technol.* **2014**, *35* (9), 1133−1139.

(66) Wang, S.; Hovland, J.; Bakke, R. Efficiency of the anaerobic digestion of amine wastes. *Biotechnol. Lett.* **2013**, *35* (12), 2051−2060.

(67) Tezel, U. *Fate and effect of quaternary ammonium compounds in biological systems*. Georgia Institute of Technology, 2009. https://smartech.gatech.edu/handle/1853/28229.

(68) Stratful, I.; Scrimshaw, M. D.; Lester, J. N. Conditions influencing the precipitation of magnesium ammonium phosphate. *Water Res.* **2001**, *35* (17), 4191−4199.

(69) Saidou, H.; Korchef, A.; Ben Moussa, S.; Ben Amor, M. Struvite precipitation by the dissolved CO_2 degasification technique: Impact of the airflow rate and pH. *Chemosphere* **2009**, *74* (2), 338−343.

(70) Hao, X.; Wang, C.; van Loosdrecht, M. C. M.; Hu, Y. Looking beyond struvite for P-recovery. *Environ. Sci. Technol.* **2013**, *47* (10), 4965−4966.

(71) Momberg, G. A.; Oellermann, R. A. The removal of phosphate by hydroxyapatite and struvite crystallisation in South Africa. *Water Sci. Technol.* **1992**, *26* (5−6), 987−996.

(72) Le Corre, K. S.; Valsami-Jones, E.; Hobbs, P.; Parsons, S. A. Impact of calcium on struvite crystal size, shape and purity. *J. Cryst. Growth* **2005**, *283* (3), 514−522.

(73) Yan, H.; Shih, K. Effects of calcium and ferric ions on struvite precipitation: A new assessment based on quantitative X-ray diffraction analysis. *Water Res.* **2016**, *95*, 310−318.

(74) Sugiyama, S.; Yokoyama, M.; Ishizuka, H.; Sotowa, K.-I.; Tomida, T.; Shigemoto, N. Removal of aqueous ammonium with magnesium phosphates obtained from the ammonium-elimination of magnesium ammonium phosphate. *J. Colloid Interface Sci.* **2005**, *292* (1), 133−138.

(75) Bhuiyan, M. I. H.; Mavinic, D. S.; Koch, F. A. Thermal decomposition of struvite and its phase transition. *Chemosphere* **2008**, *70* (8), 1347−1356.